Am J Physiol Cell Physiol
280: C962–C969, 2001.

Shear stress induces a time- and position-dependent increase in endothelial cell membrane fluidity

PETER J. BUTLER,[1,2] GERARD NORWICH,[1] SHELDON WEINBAUM,[2] AND SHU CHIEN[1]
[1]*The Whitaker Institute of Biomedical Engineering and Department of Bioengineering, University of California, San Diego, La Jolla, California 92093-0427;* [2]*Center for Biomedical Engineering and Department of Mechanical Engineering, City College of New York, New York, New York 10031*

Received 2 December 1999; accepted in final form 20 October 2000

Butler, Peter J., Gerard Norwich, Sheldon Weinbaum, and Shu Chien. Shear stress induces a time- and position-dependent increase in endothelial cell membrane fluidity. *Am J Physiol Cell Physiol* 280: C962–C969, 2001.—Blood flow-associated shear stress may modulate cellular processes through its action on the plasma membrane. We quantified the spatial and temporal aspects of the effects of shear stress (τ) on the lipid fluidity of 1,1′-dihexadecyl-3,3,3′,3′-tetramethylindocarbocyanine perchlorate [$DiIC_{16}(13)$]-stained plasma membranes of bovine aortic endothelial cells in a flow chamber. A confocal microscope was used to determine the DiI diffusion coefficient (D) by fluorescence recovery after photobleaching on cells under static conditions, after a step-τ of 10 or 20 dyn/cm^2, and after the cessation of τ. The method allowed the measurements of D on the upstream and downstream sides of the cell taken midway between the respective cell borders and the nucleus. In $<$10 s after a step-τ of 10 dyn/cm^2, D showed an upstream increase and a downstream decrease, and both changes disappeared rapidly. There was a secondary, larger increase in upstream D, which reached a peak at 7 min and decreased thereafter, despite the maintenance of τ. D returned to near control values within 5 s after cessation of τ. Downstream D showed little secondary changes throughout the 10-min shearing, as well as after its cessation. Further investigations into the early phase, with simultaneous measurements of upstream and downstream D, confirmed that a step-τ of 10 dyn/cm^2 elicited a rapid (5-s) but transient increase in upstream D and a concurrent decrease in downstream D, yielding a significant difference between the two sites. A step-τ of 20 dyn/cm^2 caused D to increase at both sites at 5 s, but by 30 s and 1 min the upstream D became significantly higher than the downstream D. These results demonstrate shear-induced changes in membrane fluidity that are time dependent and spatially heterogeneous. These changes in membrane fluidity may have important implications in shear-induced membrane protein modulation.

mechanotransduction; membrane fluidity; fluorescence recovery after photobleaching; cholesterol; alcohol

BLOOD FLOW IMPARTS ON VASCULAR endothelium a tangential shear stress, which initiates cellular processes related to vessel wall homeostasis and pathophysiology. While many cellular structures, including the cell membrane (6, 7, 13), the cytoskeleton (33), focal adhesions (10), integrins (31), and glycocalyx (18), have been proposed to respond to shear stress and initiate the cellular signaling processes, there have been few experimental attempts to quantify the direct effects of shear stress on these structures. Recent studies have suggested that at least one site of mechanotransduction may be the cell membrane via force-induced changes in fluidity (15, 18, 22).

We developed a new technique to determine the shear-induced changes in membrane fluidity at specific locations on the cell at various time intervals by measuring fluorescence recovery after photobleaching (FRAP) with a Bio-Rad 1024 confocal microscope and Time-Course software. FRAP was chosen over other methods of fluidity measurements, e.g., fluorescence polarization, electron spin resonance, and fluorescence correlation spectroscopy, because rapid measurements (temporal resolution of 1–2 s) with high spatial resolution (~2 μm) can be made. A simplified one-dimensional (1-D) model was developed to derive diffusion coefficients from the FRAP curves. The diffusion coefficient (D) of a lipophilic fluorophore is a quantitative measurement of membrane lipid fluidity (29). This novel approach of performing FRAP analysis of cells in a flow chamber led to measurements of the temporal and spatial variations of shear-induced changes in membrane-lipid fluidity, thus providing insights into mechanotransduction of shear stress by vascular endothelium.

METHODS

Cell cultures. Bovine aortic endothelial cells (BAECs) were cultured in DMEM supplemented with 2 mM L-glutamine, 50 U/ml penicillin, 50 mg/ml streptomycin, 1 mM sodium pyruvate, and 10% FCS. BAEC cultures were maintained at 37°C in a gas mixture of 95% air-5% CO_2. Cells used were from *passages 6–17*.

Serum-free DMEM containing 100 μM of the lipophilic probe, 1,1′-dihexadecyl-3,3,3′,3′-tetramethylindocarbocyanine perchlorate [$DiIC_{16}(3)$; Molecular Probes, Eugene, OR] was

Address for reprint requests and other correspondence: S. Chien, The Whitaker Institute of Biomedical Engineering and Department of Bioengineering, University of California, San Diego, 9500 Gilman Drive MC 0427, La Jolla, CA 92093-0427 (E-mail: shuchien@ucsd.edu; pbutler@be-research.ucsd.edu).

The costs of publication of this article were defrayed in part by the payment of page charges. The article must therefore be hereby marked "*advertisement*" in accordance with 18 U.S.C. Section 1734 solely to indicate this fact.

used to stain the cell membrane. The endothelial cells were washed with warm, serum-free medium, incubated at 37°C in the staining solution for 10 min, and then washed three times with serum-free medium and twice with complete medium. This procedure resulted in a uniform staining of the membrane surface as assessed by confocal microscopy (Fig. 1*B, top*). Fluidity measurements were obtained within the first 20 min after staining.

Shear stress apparatus. Immediately after staining, the glass coverslip was assembled into a parallel-plate flow chamber with dimensions of 2 mm × 5 cm × 100 μm. An infusion-withdrawal pump with adjustable rate (Harvard Apparatus, Holliston, MA) was used to induce flow through the chamber by withdrawing fluid from the downstream side of the flow chamber, with the upstream side of the flow chamber connected to a syringe barrel open to atmospheric pressure (Fig. 1*A*). A flow rate was chosen to yield a shear stress of 10 or 20 dyn/cm^2 using the equation $\tau = 6Q\mu/wh^2$, where Q is flow rate, μ is medium viscosity (0.007 poise), w is channel width, and h is channel height. Temperature was maintained at 37°C by a control loop consisting of a thermocouple, a temperature controller (Omega, Stamford, CT), and a heat gun (Master Appliance, Racine, WI) in the ultraviolet protection hood of the confocal microscope. The medium was preequilibrated with 95% air-5% CO_2 overnight in the incubator. The upstream reservoir of the flow apparatus was covered with mineral oil to maintain gas tension.

Confocal-FRAP system. BAECs were sheared at 10 or 20 dyn/cm^2 at 37°C using complete medium (DMEM with FCS). FRAP analysis was performed using a Bio-Rad 1024 confocal microscope. A thin line (0.902 μm wide) parallel to the flow direction was bleached in the otherwise uniformly fluorescent membrane midway between the nuclear region and the cell border by using repeated scans with all visible wavelengths from an argon-ion laser at 10% power (5 scans at 2 ms/scan; Fig. 1*B, bottom*). Diffusion-mediated recovery of DiI fluorescence into the bleached region was monitored using the krypton/argon laser (1% power, $\lambda_{excitation}$ = 568 nm, $\lambda_{emission}$ = 585 nm) using line scans at 2 ms/scan for up to 2 s. Diffusion coefficients were calculated by using the theory for 1-D diffusion with a Gaussian initial condition for the bleach profile and a Gaussian profile for the monitoring beam (21). The resulting equation used to fit the recovery curves was

$$\frac{f(t)}{f_i} = \frac{f_\infty}{f_i} + \left[\frac{f_0}{f_i} - \frac{f_\infty}{f_i}\right] \cdot \frac{\left[\frac{1}{L_b^2} + \frac{1}{L_m^2}\right]^{1/2}}{\left[\frac{1}{L_b^2} + \frac{(8Dt/L_b^2 + 1)}{L_m^2}\right]^{1/2}} \quad (1)$$

where t is time, f(t) is fluorescence recovery over time t , f_i = f($t < 0$) is fluorescence before bleaching, f_0 = f($t = 0$) is fluorescence immediately after bleaching, f_∞ = f($t \to \infty$) is the asymptotic value of fluorescence recovery reached in infinite time, L_b is initial Gaussian (e^{-2}) half-width of the bleached line, L_m is Gaussian half-width of the monitoring beam (krypton/argon), and D is diffusion coefficient. The details of the mathematical derivation of *Eq. 1* are given in the APPENDIX. From f_0, f_∞, and f_i we calculated the fraction of fluorophore available for diffusion, φ, where $\phi = (f_\infty - f_0)/(f_i - f_0)$.

In separate experiments we measured the profiles of the bleached line (using immobile fluorophores) and the monitoring beam [using a variation of the point-scan technique (30)]. The Gaussian (e^{-2}) half-width of the bleached line was 0.451 μm for a bleach depth similar to that induced on live cells, and the Gaussian (e^{-2}) half-width of the monitoring beam was 0.316 μm. The bleached line extended in length beyond the region of interest which was 1.7 μm in length. The slope of the membrane at the bleach location (~0.3 μm/μm) was estimated from three-dimensional reconstruction of confocal slices of DiI-stained cells (Fig. 2*B*). The error in the FRAP measurement associated with this slope is evaluated in the APPENDIX.

Experimental protocols. As positive controls, we tested the effects of a membrane fluidizing agent, benzyl alcohol (BA), and a membrane rigidifying agent, cholesterol, on endothelial cell membrane fluidity. Cells were cultured to confluence in 2 × 2-cm wells. For BA experiments, DiI-stained cells were incubated for 10 min in complete medium containing 30 mM BA (Sigma Chemicals). For cholesterol experiments, cells were incubated for 3 h in 0.1 mM cholesterol (cholesterol in methyl-β-cyclodextrin; Sigma) in complete medium and

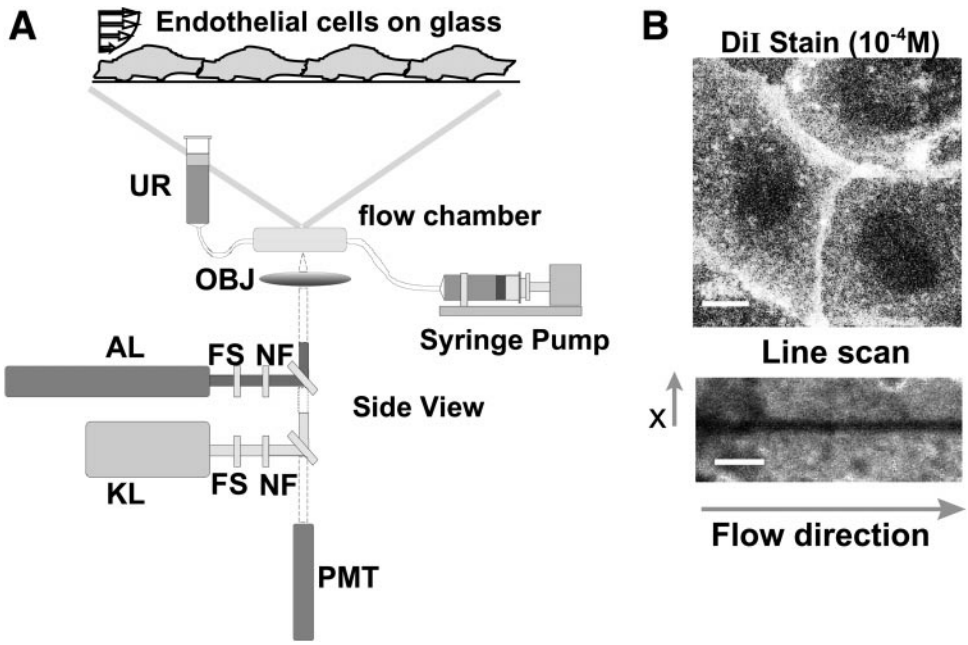

Fig. 1. *A*: confocal fluorescence recovery after photobleaching (FRAP) experimental setup. A temperature-controlled flow chamber is placed on the stage of a Bio-Rad 1024 confocal microscope. The argon-ion laser (AL) performs the bleaching event and the krypton/argon laser (KL) is used for monitoring. UR, upstream reservoir; OBJ, microscope objective; FS, fast shutter; NF, neutral density filter; and PMT, photomultiplier tube. *B*: 1,1-dihexadecyl-3,3,3′3′-tetramethylindocarbocyanine perchlorate (DiI)-stained monolayer. *Top*: DiI-stained live cells; bar = 10 μm. *Bottom*: immobile fluorophores (described in text) with a representative bleach line; bar = 3 μm. The x-coordinate originates at the midpoint of the bleached line and is perpendicular to the line. Flow direction is parallel to the bleached line.

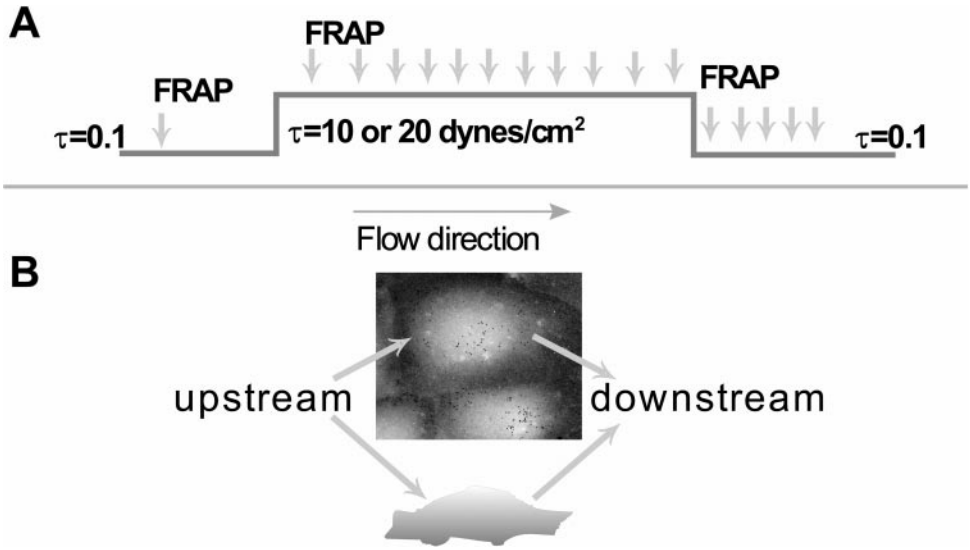

Fig. 2. Experimental protocol. *A*: FRAP measurements were made periodically on the upstream or the downstream side of the cell. *B*: the cell shape was estimated from serial reconstruction of confocal slices of the DiI-stained endothelial cells by assigning height-specific pixel values to each serial slice and then reconstructing the image (using LabVIEW image analysis software). The result is a gray-scale image in which the pixel intensities are proportional to the height above the coverslip of that part of the cell. An example is seen in the *inset* (maximum height ~5 μm). The slope of the membrane is obtained from image analysis using NIH image software and agrees with that from Barbee et al. (4). τ, shear stress.

stained with DiI. For both experiments, up to three FRAP measurements were taken per cell on multiple cells in multiple wells, all done within 3 min after staining.

To assess long-term changes in fluidity due to shear stress, periodic FRAP measurements were taken at the same spot on the cell surface over the course of the experiment (Fig. 2*A*). To assess spatial variation in shear-induced membrane fluidity, FRAP measurements were taken on the upstream side (as defined by the flow direction) or on the downstream side of the cell. The upstream and downstream positions were in the central portion of the membrane between the nucleus and the upstream or downstream cell border, respectively.

Membrane fluidity measurements were made before the step-shear of 10 dyn/cm^2, within 5 s after the step-shear, at 1-min intervals while the shear stress was maintained, immediately after the shear stress was stopped, and at 1-min intervals for 5 min thereafter. For the very-low-shear control experiments, the same measurement protocol was used but the shear stress was 0.1 dyn/cm^2.

In additional experiments to assess early fluidity changes, simultaneous measurements of upstream and downstream membrane fluidity were taken at early time points (5 s, 10 s, 30 s, 1 min, and 2 min) on cells subjected to a step-shear of 10 or 20 dyn/cm^2. Because the line scan was rapid (2 ms/scan), virtually simultaneous upstream and downstream measurements could be accomplished by bringing both regions into the field of view and selecting two regions of interest along the scan line for fluorescence monitoring.

Data and statistical analysis. D, f_0, and f_∞ were evaluated by fitting *Eq. 1* to the raw recovery data using a Levenberg-Marquardt nonlinear least-squares regression with the aid of SlideWrite software (Advanced Graphics Software, Encinitas, CA) or a custom program written in LabVIEW programming language (Fig. 3; National Instruments, Austin, TX). The diffusion coefficients for shear experiments were normalized by using the preshear value (D_{init}). These ratios (D/D_{init}) were averaged and expressed as means ± SE. For statistical analysis that involved multiple pairwise comparisons, ANOVA was performed using SigmaStat software (SPSS, Chicago, IL). For those groups showing significance among groups, the significance of differences between each experimental group was assessed using Tukey's post hoc test. For analysis of differences between simultaneous upstream and downstream fluidity measurements, upstream and downstream measurements of D/D_{init} for each cell were paired and plotted as means ± SE, and a paired t-test was used to assess significant differences at each time point. $P \leq 0.05$ was considered to be significant. In addition, 95% confidence intervals were computed for D/D_{init} for each group and each time point to assess differences from initial D/D_{init} values. All values presented in the text and figures are means ± SE.

RESULTS

Positive controls. Table 1 shows the means ± SE values of the DiI diffusion coefficients for control cells (no treatment), BA-treated cells, and cholesterol-treated cells (all without shear). Incubation of cells in 30 mM BA for 10 min resulted in a significant increase in lateral mobility of DiI in the apical membrane of BAECs over the control values. Conversely, incubation of cells in the rigidifying agent, cholesterol (0.1 mM for 3 h), resulted in a significant reduction in the DiI diffusion coefficient relative to controls. The mobile fraction ϕ was nearly 100% for control cells, and ϕ decreased slightly to 90% for BA-treated cells and to a greater extent (70%) for cholesterol-treated cells.

Effects of shear stress on membrane fluidity. For control experiments, repeated FRAP measurements

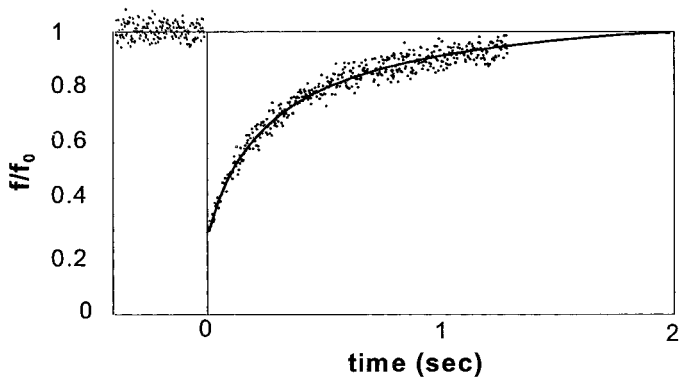

Fig. 3. Representative FRAP curve with curve fit. Data were normalized to the average prebleach fluorescence, and postbleach recovery was fitted with *Eq. 1*. Diffusion coefficient (D) = 5.34 × 10^{-9} cm^2/s. f, fluorescence.

Table 1. *Effects of BA and cholesterol on membrane fluidity of confluent BAECs*

Treatment	D, 10^{-9} cm^2/s	ϕ	n
Control	5.92 ± 0.47	0.96 ± 0.04	15
BA	7.44 ± 0.31*	0.90 ± 0.01*	26
Cholesterol	2.29 ± 0.50†	0.70 ± 0.01†	25

Values are means ± SE; n, no. of measurements. BA, benzyl alcohol; BAECs, bovine aortic endothelial cells; D, diffusion coefficient; ϕ, fraction of fluorophore available for diffusion. *$P < 0.05$, †$P < 0.001$ (vs. control).

resulted in a gradual decrease in D/D_{init} (−38% over 15 min; Fig. 4). Following the application of a step-shear stress of 10 dyn/cm^2, D/D_{init} measurements on the downstream side of the cell resulted in an abrupt decrease in fluidity followed by essentially the same time course as in the control experiments. Measurements on the upstream side of the cell, however, showed that D/D_{init} rapidly increased after step-shear, returned immediately to control values, and then began to rise by 3 min and became significantly higher than control at 7 min (D/D_{init} = 2.01 ± 0.47) after the application of step-shear. Thereafter, the D/D_{init} value decreased with time, despite the maintenance of shear stress, but remained significantly elevated over control for the 10-min duration of shear. On cessation of shear stress, D/D_{init} returned to near control values. While the earliest changes in upstream and downstream D/D_{init} were not significantly different from control values, they were significantly different from each other as assessed by ANOVA and a Tukey's post hoc pairwise comparison. The mobile fraction of cells subjected to shear, as for the control cells, was ~100% in all cases.

To investigate the possible early changes in fluidity, we performed additional FRAP measurements at 5 s, 10 s, 30 s, 1 min, and 2 min on the upstream and downstream sides of the cell after the application of step-shears of 10 or 20 dyn/cm^2. In these experiments, fluorescence recovery was measured simultaneously in the upstream and downstream parts of the cell by putting both areas in the field of view for nearly simultaneous measurements. Consistent with the first set of experiments, a step-shear of 10 dyn/cm^2 caused a slight increase in D (D/D_{init}= 1.15 ± 0.13) at 5 s, which was significantly higher than the downstream value (D/D_{init}= 0.88 ± 0.08; Fig. 5*A*). These shear-induced differences in D vanished by 10 s. A step-shear stress of 20 dyn/cm^2 elicited an early increase (5 s) in membrane fluidity that was greater on the upstream (D/D_{init} = 1.45 ± 0.13) than downstream side (D/D_{init} = 1.16 ± 0.09; Fig. 5*B*), although this difference was not significant. On the downstream side of the cell, the initial increase rapidly disappeared to control levels by 10 s while the upstream diffusion coefficient remained elevated for up to 1 min. The upstream D/D_{init} was significantly different from the downstream D/D_{init} at the 30-s and 1-min time points (Fig. 5*B*). This upstream D/D_{init} returned to initial values by 2 min (Fig. 5*B*).

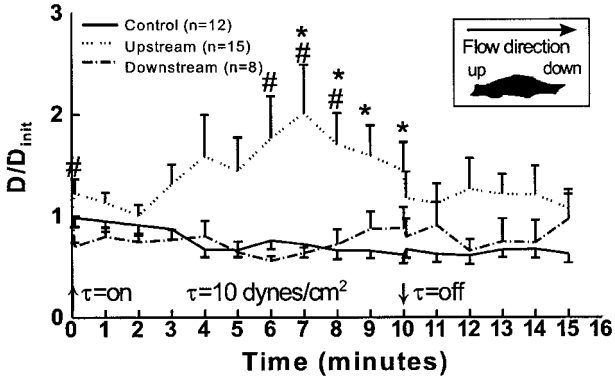

Fig. 4. Long-term shear-induced changes in fluidity. Increases in fluidity due to the application of a step-shear of 10 dyn/cm^2 at *time 0* occurred only on the upstream side of the cell. Measurements on upstream and downstream parts of cells were performed on different cells from different experiments. *Significant difference between upstream and control values. #Significant difference between upstream and downstream values ($P \leq 0.05$).

DISCUSSION

In the present study we demonstrate that a confocal laser scanning microscope can be used to perform simultaneous, multipoint FRAP measurements with three-dimensional spatial specificity. We confirmed the utility of this system through rigorous comparisons with more specialized FRAP systems (see discussion below) and by showing that BA and cholesterol cause an increase and decrease, respectively, of endothelial

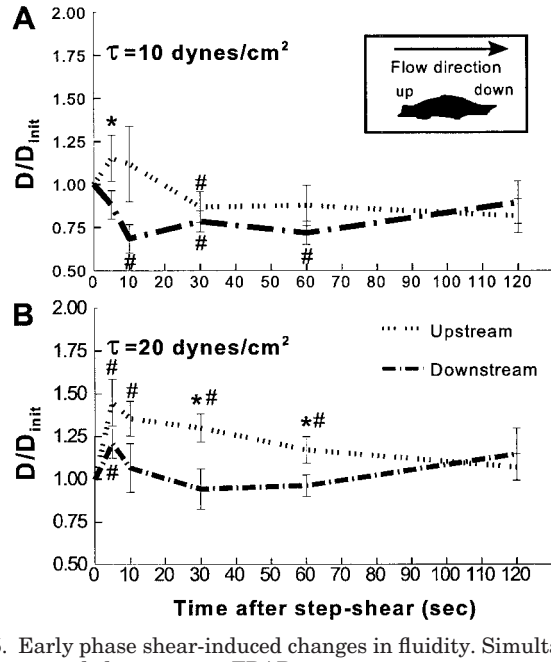

Fig. 5. Early phase shear-induced changes in fluidity. Simultaneous upstream and downstream FRAP measurements were made and paired for each cell. Error bars on the D/D_{init} vs. time graphs are the mean D/D_{init} ± SE. *Significant difference between upstream and downstream values as assessed by a paired t-test ($P \leq 0.05$). #Significant difference from 1 as assessed by 95% confidence intervals. *A*: upstream and downstream D/D_{init} values at 0, 5, 10, 30, 60, and 120 s after the application of a step-shear of 10 dyn/cm^2 (n = 9). *B*: upstream and downstream D/D_{init} values at 0, 5, 10, 30, 60, and 120 s after the application of a step-shear of 20 dyn/cm^2 (n = 8).

cell membrane fluidity in terms of DiI diffusion coefficient D. We used this system to measure the time course and spatial distribution of shear-induced changes in membrane fluidity. The main findings of the present study are as follows: *1*) a shear stress of 10 dyn/cm^2 was sufficient to induce both early (5 s) and delayed (>5 min) increases in D; *2*) this moderate shear of 10 dyn/cm^2 elicited an increase and decrease in up- and downstream D, respectively, with the change being rapid and transient; *3*) a higher shear stress of 20 dyn/cm^2 caused increases in both up- and downstream D, with the upstream increase being greater and more sustained than the downstream increase; and *4*) the upstream increases in D resulting from a step-shear of 20 dyn/cm^2 were sustained for a longer period than those resulting from 10 dyn/cm^2.

Shear stress initiates many cellular processes ranging from immediate changes in ion conductance and G protein activation (seconds) to alterations in cytoskeletal organization and gene expression (minutes to hours) (9). The most proximal events mediating this mechanotransduction have not been clearly established and may occur via multiple structures. Furthermore, long-term effects of shear stress may be transduced by signaling pathways and cellular structures different from those mediating the immediate events. One logical candidate for a mechanotransducer is the cell membrane because of its proximity to the flowing blood. It was the goal of the present study to measure the direct effects of shear stress on the cell membrane fluidity, a property that has been shown to be strongly correlated with cell functions [by modifying membrane protein diffusion (1) and function (11)]. Membrane fluidity has been proposed as a modulator of shear-related cellular processes (11, 18), and, recently, Haidekker et al. (17) published results on an early increase in membrane fluidity due to shear stress. To our knowledge, the present study represents the first experimental quantification of the temporal (short-term and long-term) and spatial (upstream vs. downstream) aspects of shear-induced increases in fluidity on the apical plasma membrane.

To assess diffusion of unbleached fluorophore into a bleached line, we solved the 1-D diffusion equation (2, 20). The effects of convection of fluorophores via lipid flow or of cell deformation in the direction of flow on the FRAP measurements were neglected, because the lines were made parallel to the flow direction. The membrane where the FRAP measurement was made was considered flat and devoid of corrugations and/or microvilli (see APPENDIX for estimation of the error associated with the assumption of a flat membrane). To measure the initial bleach geometry, we performed the bleaching experiments on fluorophores made immobile by drying the stained cells and then returning them to culture medium. We measured the beam shape using a variation of the point scan method (30) by scanning a laser past a small stationary (0.17-μm diameter) fluorescent latex microsphere (Molecular Probes) and then fitting the fluorescent profile with a Gaussian curve. Alignment of bleaching and monitoring lasers was verified each day by projecting the beams through a target-labeled prism mounted on the microscope nose piece. Finally, we compared the ability and accuracy of our model to assess D with that of Stolpen et al. (32), who bleached with an extended elliptical beam to approximate a line bleach. For the same D, f_0/f_i, f_∞/f_i, L_b, and L_m, fluorescence recovery curves generated by our model agreed with those generated by Stolpen et al. within 4%. While 46 terms were summed in their model for this comparison, our model does not require any summation and hence is convenient for curve fitting using standard curve-fitting software.

We report that both physiologically moderate (10 dyn/cm^2) and high (20 dyn/cm^2) shear stress elicits a significant immediate (5 s) increase in membrane fluidity as measured by FRAP. This increase subsided by 10 s for 10 dyn/cm^2 and by 2 min for 20 dyn/cm^2. The transient nature of the response suggests that the early increase in membrane fluidity is in response to the sudden onset of shear and that this response is dissipated. Recently, Haidekker et al. (17), using a molecular rotor, 9-(dicyanovinyl)-julolidine (DCVJ), to assess membrane fluidity, also showed an increase in fluidity by 5 s after step-shear, but there the increase in fluidity was found to be sustained. The reason for the differences in persistence of this early change is not clear at this time but may be due to differences in cell types (human umbilical vein endothelial cells vs. BAECs) or perfusion medium (Hanks' balanced salt solution vs. DMEM-FCS), or methods of measurement (DCVJ fluorescence vs. FRAP). The DCVJ measurement represents fluidity averaged over the entire cell culture, whereas our FRAP measurement was localized to specific subcellular regions on the cell membrane observed under confocal microscopy. In any event, the present data support, as did Haidekker et al., the suggestion that membrane fluidity may play a role in modulating some of the earliest events known to be related to the mechotransduction of shear stress (e.g., G protein hydrolysis, ion channel conductance).

Simultaneous upstream and downstream measurements of DiI diffusion revealed a spatial distribution of the effects of shear stress on the membrane, and the magnitude and persistence of the change were related to the level of shear stress. A shear stress of 10 dyn/cm^2 caused a rapid (5 s) increase and decrease in DiI diffusion on the upstream and downstream portions of the membrane, respectively, and both returned to initial values by 10 s. A step-shear of 20 dyn/cm^2, however, caused increases in DiI diffusion on both the upstream and downstream parts of the cell, with the upstream increase persisting for 1 min and the downstream increase falling to initial values by 10 s. These differences in spatial distribution and persistence of the shear-induced increases in fluidity may provide insights into how the cell can sense differences in shear magnitude.

This novel finding that the increase in membrane fluidity is predominantly found in the upstream side of the cell correlates well with the location of positive shear stress gradient distributions, which were com-

puted by Barbee et al. (5), but not with the absolute shear stress distributions. Using measured cell topography and computational fluid dynamics, Barbee et al. showed that shear stress is symmetrically distributed on the upstream and downstream side of the cell, whereas positive temporal shear stress gradients are concentrated on the upstream side of the cell. Hence our observation that shear stress induced a differential spatial (upstream vs. downstream) change in membrane fluidity suggests that shear stress gradients, in addition to shear stress per se, may play an important role in modulating membrane fluidity.

The results here, demonstrating a delayed (>5 min) increase in membrane fluidity, also support the hypothesis that the membrane fluidity, as measured by DiI-FRAP, may play a role in modulating later responses to shear stress. The only other study to investigate the later perturbing effects of shear stress on the cell membrane was performed by Berthiaume and Frangos (6), who used the shear-induced incorporation of MC540 (a lipophilic dye) into the endothelial cells to reflect an increase in membrane permeability. They found a significant increase in the incorporation of the dye beginning at 5 min after shearing with medium 199 supplemented with 20% FCS. Our results on the time course of fluidity changes with shear stress are in excellent agreement with theirs on the shear-induced incorporation of this lipophilic dye.

The causes of shear-induced increases in membrane fluidity remain unclear. It is likely that fluid shear would cause a time-dependent cell deformation in the direction of flow, thus leading to temporally varying and spatially heterogeneous stresses in the cell membrane. These may, in turn, induce time- and position-dependent fluidity changes. In support of this hypothesis, Sato et al. (28) showed that, when endothelial cells are suctioned with a small pipette, a portion of the cell exhibits an immediate elastic deformation followed by a slower viscous deformation. The time scales of these deformations agree well with the early and late increases in membrane fluidity shown in the present study. Wang et al. (34), modeling cell deformation with shear stress, have suggested that shear causes the nuclear bulge to deform in the direction of flow. Such deformation may lead to increased tension in the upstream cell membrane. Experimental support of such cell deformation has been given by Helmke et al. (19), who showed that intermediate filaments close to the apical membrane are displaced in the direction of flow within the first 3 min after the application of a step-shear stress. Finally, the link between membrane strain and membrane fluidity is suggested by the increase in membrane fluidity of human fibroblasts in response to hypotonic swelling (3).

Physiological processes in the cell may be caused by increases in membrane fluidity. Prostacyclin production has been shown to be enhanced by an increase in membrane fluidity (3). Hence, the increases in fluidity after a step-shear observed here may partially explain the prostaglandin-mediated vasodilation seen in our recent study (8). The physiological implications of the more sustained component of increases in membrane fluidity shown here are suggested by a study in which cell apoptosis was caused by agents that induced a sustained increase in membrane fluidity (12).

The cytoskeleton may modulate membrane dynamics. There is evidence that actin filaments remodel on the time scale of the later fluidity changes seen in this study (23). Morita et al. (24) showed that a low shear stress of 5 dyn/cm^2 could elicit the depolymerization of F-actin to G-actin in as early as 5 min. Although the shear-induced actin depolymerization is not expected to alter membrane fluidity directly (29), it is likely to alter cell deformation with flow (25). In an earlier study from our laboratory, Galbraith et al. (14) noted that microtubule remodeling due to shear stress occurred preferentially in the upstream side of the cell, and Hage Chahine et al. (16) showed that microtubule disassembly increases membrane fluidity of fibroblasts as measured with FRAP. Finally, Sato et al. (27) noted that the cell surface was stiffer on the upstream side of the cell after 6 h of flow and attributed this polarization to localized stress fiber development. Together, these studies suggest that the cytoskeleton has an intimate association with the membrane and may modulate its functions via membrane stabilization/destabilization cycles.

In summary, we have introduced a novel quantitative measurement of the temporal changes in membrane fluidity and its spatial distribution in response to shear stress. The time course and heterogeneous distribution of the increase in fluidity with shear stress may be related to calcium signaling, shear-induced phospholipid metabolism, and cytoskeletal remodeling. Fluidity changes are likely to have a significant effect on membrane proteins and their interactions (1, 26).

APPENDIX

FRAP Model

The following model describes isotropic, 1-D diffusion into a bleached line with a Gaussian profile initial condition. We first write the 1-D diffusion equation

$$\frac{\partial c}{\partial t} = D\left(\frac{\partial^2 c}{\partial x^2}\right), \text{ I.C. } c_0(x) = c_\infty + [c_0(0) - c_\infty](1 - e^{-2x^2/L_b^2}), \quad \text{B.C. } \frac{\partial c}{\partial x}\Big|_{x=0} = 0,\ c(x \to \infty) = c_\infty \tag{A1}$$

where c is concentration of unbleached fluorophore, t is time, x is coordinate perpendicular to the bleached line, D is diffusion coefficient, and L_b is Gaussian half-width of the bleach line. IC is the initial condition, and BC is the boundary condition. The solution is (using Fourier analysis)

$$c(x, t) = c_\infty + [c_0(0) - c_\infty]\frac{1}{\sqrt{8\frac{Dt}{L_b^2} + 1}} \exp\left(\frac{-2\frac{x^2}{L_b^2}}{8\frac{Dt}{L_b^2} + 1}\right) \tag{A2}$$

To obtain the fluorescence (f) from these concentration profiles, we integrate the product of the concentration and the

monitor beam intensity profile (I_m) over the confocal aperture distance (a). In other words

$$f(t) = 2\int_0^a I_m(x)c(x,t)dx \text{ where: } I_m(x) = I_{m0}\cdot\exp\left(-2\frac{x^2}{L_m^2}\right) \quad (A3)$$

where I_{m0} is the peak intensity and L_m is the Gaussian beam radius for the monitoring beam. The solution to *Eq. A3* is

$$f(t) = 2I_{m0}c_\infty + [2I_{m0}c_0(0) - 2I_{m0}c_\infty] \cdot \frac{1}{\sqrt{2}}\left[\frac{1}{L_b^2} + \frac{(8Dt/L_b^2 + 1)}{L_m^2}\right]^{-1/2} \cdot \text{erf}\left[a\frac{\sqrt{2}}{\sqrt{8Dt/L_b^2 + 1}}\cdot\left(\frac{1}{L_b^2} + \frac{(8Dt/L_b^2 + 1)}{L_m^2}\right)\right] \quad (A4)$$

To simplify *Eq. A4* we solve for $f(t\to\infty) = f_\infty$ and $f(t = 0) = f_0$ and recognize that the error function, erf(∞), approaches 1. Because a (the confocal aperture distance) is large, the erf term goes to 1 and *Eq. A4* simplifies to

$$f(t) = f_\infty + (f_0 - f_\infty)\cdot\frac{\left(\frac{1}{L_b^2} + \frac{1}{L_m^2}\right)^{1/2}}{\left[\frac{1}{L_b^2} + \frac{(8Dt/L_b^2 + 1)}{L_m^2}\right]^{1/2}} \quad (A5)$$

which, when normalized to the initial fluorescence, becomes *Eq. 1* in the text.

The error associated with the assumption of a flat membrane can be estimated by using the slope of the membrane, the length of the region of interest for fluorescence measuring, and the depth of the confocal field. If the membrane has a slope of 0.3 μm/μm (see Fig. 2 and Ref. 4), and the region of interest (ROI) is 1.7 μm long, then the left and right edges of the ROI will be out of the focal plane by 0.25 μm. (Note that the bleached line is longer than the ROI and, therefore, there is no diffusion of fluorophores from the upstream and downstream edges of the ROI). The depth of the confocal field for a ×60 1.4 numerical aperture (NA) objective is ~0.61 μm (14), or 0.3 μm above and below the center of the ROI. The error arises from the broadening of the laser beam with distance from the focal point and the consequent broadening of L_b and L_m. From the definition of numerical aperture, NA= 1.5 sin θ (where 1.5 is the refractive index of the immersion oil, θ is the half angle subtended by the laser beam, and NA = 1.4), we can estimate that the beam will broaden by ~0.1 μm at 0.3 μm from the focal point. We then compute the area increase for the bleaching and monitoring beams and compute effective L_m and L_b that yield the effective areas. These widths are 0.476 μm for the bleaching beam and 0.340 μm for the monitoring beam. Replacing L_b and L_m with these values yields an ~12% underestimation of D for control values and an ~10% underestimation of the peak values of D. When normalized, these errors yield an ~4% overestimation of the twofold increase seen on the upstream side at 7 min after a step-shear stress of 10 dyn/cm^2.

We thank Dr. Jeffrey H. Price, of the National Science Foundation-Whitaker Quantitative Imaging and Confocal Microscopy Resource at University of California San Diego for assistance in confocal microscopy and valuable suggestions regarding FRAP, and we thank Dr. Shunichi Usami for expert technical advice and assistance.

This work was supported by National Heart, Lung, and Blood Institute Grants HL-19454 and HL-43026.

P. J. Butler is a recipient of an National Institutes of Health National Research Service Award.

REFERENCES

1. **Axelrod D.** Lateral motion of membrane proteins and biological function. *J Membr Biol* 75: 1–10, 1983.
2. **Axelrod D, Koppel DE, Schlessinger J, Elson E, and Webb WW.** Mobility measurement by analysis of fluorescence photobleaching recovery kinetics. *Biophys J* 16: 1055–1069, 1976.
3. **Baciulis V, Luthy C, Hofer G, Toplak H, Wiesmann UN, and Oetliker OH.** Specific and nonspecific stimulation of prostaglandin release by human skin fibroblasts in culture. Are changes of membrane fluidity involved? *Prostaglandins* 43: 293–304, 1992.
4. **Barbee KA, Davies PF, and Lal R.** Shear stress-induced reorganization of the surface topography of living endothelial cells imaged by atomic force microscopy. *Circ Res* 74: 163–171, 1994.
5. **Barbee KA, Mundel T, Lal R, and Davies PF.** Subcellular distribution of shear stress at the surface of flow-aligned and nonaligned endothelial monolayers. *Am J Physiol Heart Circ Physiol* 268: H1765–H1772, 1995.
6. **Berthiaume F and Frangos JA.** Fluid flow increases membrane permeability to merocyanine 540 in human endothelial cells. *Biochim Biophys Acta* 1191: 209–218, 1994.
7. **Busse R, Mülsch A, Fleming I, and Hecker M.** Mechanisms of nitric oxide release from the vascular endothelium. *Circulation* 87, *Suppl* 5: V18–V25, 1993.
8. **Butler PJ, Weinbaum S, Chien S, and Lemons DE.** Endothelium-dependent, shear-induced vasodilation is rate-sensitive. *Microcirculation* 7: 53–65, 2000.
9. **Davies PF.** Flow-mediated endothelial mechanotransduction. *Physiol Rev* 75: 519–560, 1995.
10. **Davies PF, Robotewskyj A, and Griem ML.** Quantitative studies of endothelial cell adhesion. Directional remodeling of focal adhesion sites in response to flow forces. *J Clin Invest* 93: 2031–2038, 1994.
11. **Frangos JA and Gudi S.** Shear stress activates reconstituted G-proteins in the absence of protein receptors by modulating lipid bilayer fluidity (Abstract). *FASEB J* 11: A521, 1997.
12. **Fujimoto K, Iwasaki C, Kawaguchi H, Yasugi E, and Oshima M.** Cell membrane dynamics and the induction of apoptosis by lipid compounds. *FEBS Lett* 446: 113–116, 1999.
13. **Fung YC and Liu SQ.** Elementary mechanics of the endothelium of blood vessels. *J Biomech Eng* 115: 1–12, 1993.
14. **Galbraith CG, Skalak R, and Chien S.** Shear stress induces spatial reorganization of the endothelial cell cytoskeleton. *Cell Motil Cytoskeleton* 40: 317–330, 1998.
15. **Gudi S, Nolan JP, and Frangos JA.** Modulation of GTPase activity of G proteins by fluid shear stress and phospholipid composition. *Proc Natl Acad Sci USA* 95: 2515–2519, 1998.
16. **Hage Chahine JM, Cribier S, and Devaux PF.** Phospholipid transmembrane domains and lateral diffusion in fibroblasts. *Proc Natl Acad Sci USA* 90: 447–451, 1993.
17. **Haidekker MA, L'Heureux N, and Frangos JA.** Fluid shear stress increases membrane fluidity in endothelial cells: a study with DCVJ fluorescence. *Am J Physiol Heart Circ Physiol* 278: H1401–H1406, 2000.
18. **Hecker M, Mulsch A, Bassenge E, and Busse R.** Vasoconstriction and increased flow: two principal mechanisms of shear stress-dependent endothelial autacoid release. *Am J Physiol Heart Circ Physiol* 265: H828–H833, 1993.
19. **Helmke BP, Goldman RD, and Davies PF.** Rapid displacement of vimentin intermediate filaments in living endothelial cells exposed to flow. *Circ Res* 86: 745–752, 2000.
20. **Jacobson K.** Lateral diffusion in membranes. *Cell Motil* 3: 367–373, 1983.
21. **Jain RK, Stock RJ, Srikanth RC, and Rueter M.** Convection and diffusion measurements using fluorescence recovery after photobleaching and video frame analysis: in vitro calibration and assessment. *Microvasc Res* 39: 77–93, 1990.
22. **Knudsen HL and Frangos JA.** Role of cytoskeleton in shear stress-induced endothelial nitric oxide production. *Am J Physiol Heart Circ Physiol* 273: H347–H355, 1997.

23. **McGrath JL, Tardy Y, Dewey CFJ, Meister JJ, and Hartwig JH.** Simultaneous measurements of actin filament turnover, filament fraction, and monomer diffusion in endothelial cells. *Biophys J* 75: 2070–2078, 1998.
24. **Morita T, Kurihara H, Maemura K, Yoshizumi M, Nagai R, and Yazaki Y.** Role of Ca^{2+} and protein kinase C in shear stress-induced actin depolymerization and endothelin 1 gene expression. *Circ Res* 75: 630–636, 1994.
25. **Pourati J, Maniotis A, Spiegel D, Schaffer JL, Butler JP, Fredberg JJ, Ingber DE, Stamenovic D, and Wang N.** Is cytoskeletal tension a major determinant of cell deformability in adherent endothelial cells? *Am J Physiol Cell Physiol* 274: C1283–C1289, 1998.
26. **Saffman PG and Delbruck M.** Brownian motion in biological membranes. *Proc Natl Acad Sci USA* 72: 3111–3113, 1975.
27. **Sato M, Nagayama K, Kataoka N, Sasaki M, and Hane K.** Local mechanical properties measured by atomic force microscopy for cultured bovine endothelial cells exposed to shear stress. *J Biomech* 33: 127–135, 2000.
28. **Sato M, Ohshima N, and Nerem RM.** Viscoelastic properties of cultured porcine aortic endothelial cells exposed to shear stress. *J Biomech* 29: 461–467, 1996.
29. **Schlessinger J, Axelrod D, Koppel DE, Webb WW, and Elson EL.** Lateral transport of a lipid probe and labeled proteins on a cell membrane. *Science* 195: 307–309, 1977.
30. **Schneider MB and Webb WW.** Measurement of submicron laser beam radii. *Appl Optics* 20: 1382–1388, 1981.
31. **Shyy Y-J, and Chien S.** Role of integrins in cellular responses to mechanical stress and adhesion. *Curr Opin Cell Biol* 9: 707–713, 1997.
32. **Stolpen AH, Golan DE, and Pober JS.** Tumor necrosis factor and immune interferon act in concert to slow the lateral diffusion of proteins and lipids in human endothelial cell membranes. *J Cell Biol* 107: 781–789, 1988.
33. **Wang N, Butler JP, and Ingber DE.** Mechanotransduction across the cell surface and through the cytoskeleton. *Science* 260: 1124–1127, 1993.
34. **Wang X, Wache P, Maurice G, Muller S, Lucius M, and Stoltz JF.** Two-dimensional simulation of the deformation of a model endothelial cell in a laminar flow. *Proceedings of the First Joint BMES/EMBS Conference: Serving Humanity Advancing Technology, Oct. 13–16, 99, Atlanta, Ga, USA,* edited by Blanchard SM. Piscataway, NJ: IEEE, 1999, p. 1341.